Fibers and Polymers 2013, Vol.14, No.4, 518-524 DOI 10.1007/s12221-013-0518-4

Interfacial Localization of Multiwalled Carbon Nanotubes in Immiscible Blend of Poly(ethylene terephthalate)/Polyamide 6

Jing Zhou and Byung Gil Min*

Department of Materials Design Engineering, Kumoh National Institute of Technology, Gumi 730-701, Korea
(Received December 5, 2012; Revised January 8, 2013; Accepted January 11, 2013)

Abstract: In this study, multiwalled carbon nanotubes (MWCNTs) were confined or localized in an immiscible blend of poly(ethylene terephthalate)/polyamide 6 (PET/PA6). A co-rotating twin-screw extruder and melt-compounding were used to prepare nanocomposites of PET/PA6 (60/40, w/w) and MWCNTs with various MWCNT contents in the range 0.001-2 phr. The raw, unfunctionalized MWCNTs were used as fillers. A remarkable change in the morphology of the blend happened on the basis of the amount of MWCNTs added to the blend: the PET phase converted into the PA6 phase at a certain MWCNT content. Although the PA6 phase was formed as a domain phase in the PET matrix in blends containing less than 0.01 phr of MWCNTs, the PET phase suddenly became discontinuous because of phase conversion in the PA6 matrix in blends containing 0.01 and 0.05 phr of MWCNTs. In the blends containing more than 0.1 phr of MWCNTs, the initial morphology was recovered, that is, the PET phase became the matrix phase again. Moreover, in the recovered state, the of the PA6 domain was much larger in the blends containing more than 0.1 phr of MWCNTs than it was in the composites that did not contain any MWCNTs and in those that contained 0.001 phr of MWCNTs. The MWCNTs, on the other hand, selectively located at the interface of the PET and PA6 phases. The rheological, electrical, and crystallization behaviors of the blends were also investigated to study the effects of the concentration of MWCNTs on the structure of the prepared composites.

Keywords: Poly(ethylene terephthalate), Polyamide 6, Polymer blends, Carbon nanotubes, Selective localization

Introduction

Since Iijima's report in 1991 [1], carbon nanotubes (CNTs) have been widely used in various fields owing to their remarkable mechanical, thermal, and electrical properties [2-4]. Using polymeric nanocomposites containing CNTs is an economical and effective way to develop polymeric materials with improved mechanical and/or electrical properties [5-7].

Polymer blends produced with CNTs have received more attention than single-component polymeric nanocomposites produced with CNTs in the past decade. CNT localization in a polymer blend is a crucial factor that affects the properties of polymeric nanocomposites produced with CNTs [8-10]. CNTs usually either selectively locate at one polymer component or diffuse throughout all polymer components [11-15]. However, the literature has rarely reported CNTs located at the interfaces of polymer blends. Yan *et al*. [16] reported that multiwalled carbon nanotubes (MWCNTs) could be selectively localized at the interface of polyamide 6/polystyrene (PA6/PS) blends through *in-situ* polymerization of styrene and ε-caprolactam in the presence of MWCNTs. Bose *et al*. [17] studied blends of PA6 and acrylonitrile-butadiene-styrene (ABS) in the presence of styrene-maleic anhydride (SMA) copolymer and MWCNTs. The MWCNTs appeared to locate at the interface because they were chemically coupled with SMA compatibilizer, which is located at the interface. Baudouin *et al*. [18] found that CNTs migrated to the interface because of thermodynamic force in immiscible polymer blends of a functionalized polyethylene and either a polyamide 6 or a polyamide 12. They also reported that the CNTs similarly localized at the interface in the immiscible polymer blends of polyamide and ethylene-acrylate (EA) copolymer [19].

Poly(ethylene terephthalate) (PET) is widely used to produce fibers, films, and bottles. PA6, on the other hand, is used as engineering plastic for various automotive parts and other applications such as various fibers. PET and PA6 each have an advantage for application to synthetic fibers. For example, PET is cheaper and has higher thermal properties than PA6, and PA6 has higher moisture absorption than PET. As the polymers are immiscible, however, there have previously been trials involving the use of compatibilizers such as epoxy [20], ionomer (Ion., Zn^{2+}) [21], nano-SiO_2 [22], or ethylene-acrylate-(maleic anhydride) terpolymer (E-AE-MA) [24] to enhance the mechanical properties of the PET/PA6 alloys. However, there have not been any reports on CNT localization in PET/PA6 blends.

In this study, the localization behavior of MWCNTs and effects of MWCNTs on the morphology and on the rheological, electrical, and crystallization properties of PET/PA6 blends produced using melt-compounding with very low amounts (0.001-2 phr) of MWCNTs were investigated.

Experimental

Materials

PET (Intrinsic Viscosity: 0.82 dl/g) and PA6 (Relative Viscosity: 2.45) chips were provided by Woongjin Chemical Co., Ltd. (Korea) and Rhodia Polyamide Co., Ltd. (Korea), respectively. MWCNTs (CM-95, purity=90 %, diameter=

*Corresponding author: bgmin@kumoh.ac.kr

10-15 nm) were purchased from Iljin Nanotech Co., Ltd. (Korea). The MWCNTs were used without further purification or functionalization. Formic acid (above 99 %) used for etching was purchased from Daejung Chemicals and Metals Co., Ltd. (Korea).

Preparation of Nanocomposites

Before the components were melt-compounded, they were all dried under vacuum at 80 °C for 24 h. The MWCNTs and both types of polymer chips were premixed using a programmable ball mill (Daihan Scientific Co., Korea), so that the MWCNTs would homogeneously adhere to the surface of the polymer chips. Although the blend ratio of PET/PA6 was fixed at 60/40 (w/w), the MWCNT content in the blends was varied among 0, 0.001, 0.01, 0.05, 0.1, 0.3, 0.5, 1, and 2 phr. The premixtures were then melt-compounded using a co-rotating twin-screw extruder (BK-11, Bowtek Co., Korea). The screw length and diameter of the extruder were 440 and 11 mm, respectively. The temperature profile for the extruder from Zone 1 (hopper) to Zone 6 was controlled in the range 180-220-240-260-270-280 °C for Zones 1-2-3-4-5-6, respectively. The extruded strands were cooled in a water bath, chopped into pellets, and dried under vacuum at 80 °C for 24 h.

Characterization of Nanocomposites

The morphologies of the blend and the nanocomposites were observed using scanning electron microscopy (SEM, JSM-6380LV, JEOL). Before SEM observation, the extruded strands were cryofractured using liquid nitrogen. Moreover, the PA6 phase in the blends was selectively etched out by dipping the strands in formic acid to observe the separation of the PET and PA6 phases.

Localization of the MWCNTs in the blends was examined using transmission electron microscopy (TEM, JEM 2100, JEOL). A cryoultramicrotome (Model: PTPC & CRX, RMC) equipped with a diamond knife was used to prepare ultrathin sections of the strands for TEM analysis.

The surface resistivity of PET/PA6/CNT nanocomposite blends was measured using a source meter (Model: 6517A Electrometer, Keithley) for the hot-pressed 0.3-mm-thick composite films. The measurement device was interfaced with a computer to record and process the data.

The melt-flow index (MFI) of the nanocomposite blends was measured using a melt indexer (Model: MP600, Tinius Olsen, Inc.) at 260 °C according to the ASTM D1238 standard. The apparent viscosity was calculated from the MFI data according to the ASTM D3835 standard.

The crystallization behavior of the nanocomposite blends was investigated using a differential scanning calorimeter (DSC, Model: Diamond DSC, PerkinElmer, Inc.). The samples were maintained at 280 °C for 5 min to erase the thermal history and were then cooled to –20 °C at a rate of 10 °C/min under a nitrogen gas flow.

Results and Discussion

Effect of MWCNT Content on Morphologies of Nanocomposite Blends

SEM and TEM were used to investigate the morphology of the PET/PA6 (60/40) blend in order to detect the locations of the MWCNTs in the blend. Figure 1 shows the effect of MWCNTs on the phase separation of the PET/PA6 blend. Because the PA6 component in the blends was etched out before the samples were observed using SEM and TEM, the dark area in the images represents the PA6 phase.

Figure 1(a) shows sea-island-type phase separation in the neat PET/PA6 blend (60/40, w/w). In the neat blend, the PA6 minor component formed a discontinuous domain with an average diameter of 0.7 μm m in a continuous PET phase, as expected from the immiscibility of the PET and PA6 components. Although an ester-amide exchange reaction happens in PET/PA6 blends (resulting in improved component compatibility) [24], clear phase separation was still observed in the blends prepared under the melt-compounding conditions used in this study. The morphology of the blend containing 0.001 phr of MWCNTs did not significantly change, as shown in Figure 1(b). However, the morphologies of the blends containing 0.01 and 0.05 phr of MWCNTs dramatically changed, as shown in Figures 1(c) and (d), respectively. It is very interesting that the phases in the blend inverted when a small amount of MWCNTs was added to the blend (Because the PA6 phase was etched out before the samples were observed using SEM and TEM, the discontinuous domain phase appearing in the images corresponds to the PET component). Another interesting phenomenon that occurred is that the initial state of phase separation was recovered for the blends containing more than 0.1 wt% of MWCNTs, as exhibited in Figures 1(e-i). Thus, the PA6 phase forms a domain in the PET matrix. In the nanocomposite blends containing more than 0.1 wt% of MWCNTs, the size of the PA6 domain showed a maximum for the blend containing 0.1 wt% of MWCNTs and decreased with increasing of MWCNT content. We assume that the interface-located MWCNTs had a compatibilizing effect on the PET/PA6 blends and caused the interfacial tension of the blends to change.

Location of MWCNTs in Nanocomposites

TEM analysis was used to determine the location of the MWCNTs in the nanocomposite blends. Figures 2(a) and (b) show the TEM images of the nanocomposites containing 0.01 and 0.1 phr of MWCNTs, respectively. The MWCNTs are clearly localized at the interface between the PET and PA6 phases.

Figure 3 shows the SEM micrographs of the cryofractured nanocomposite blend containing 0.5 phr of MWCNTs. Figures 3(a) and (b) display the surface of PA6 nodules and the cavities in the matrix formed during cryofracture. From

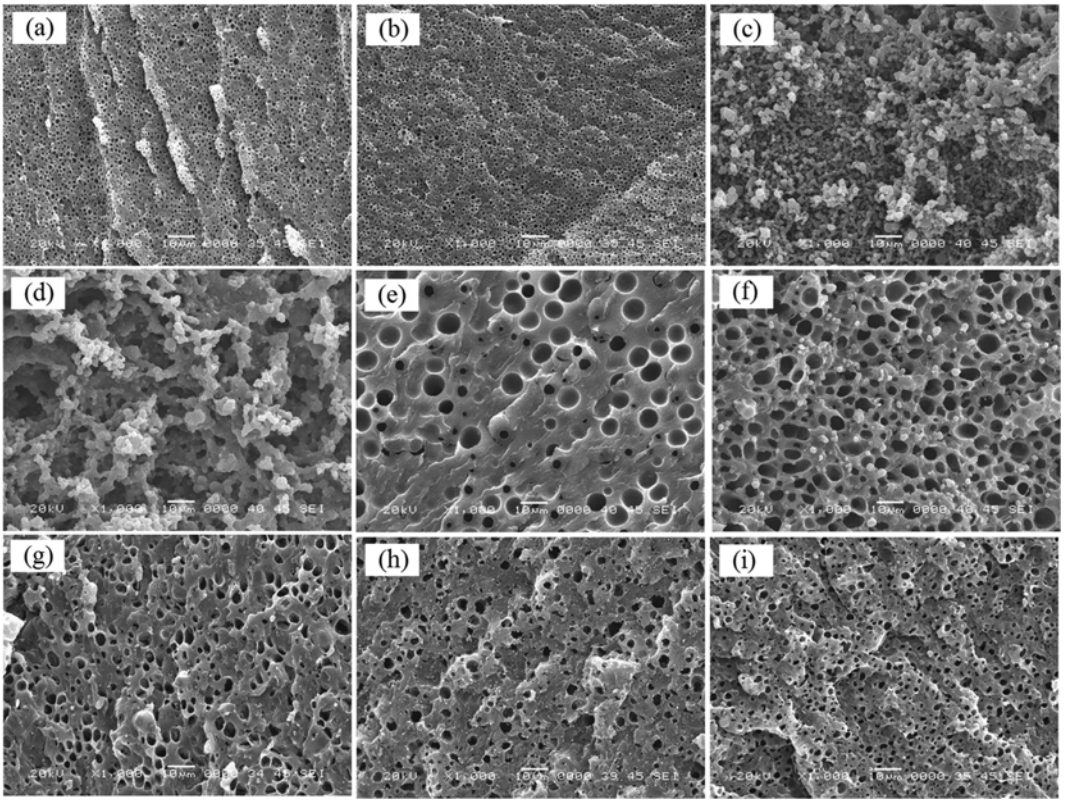

Figure 1. SEM images of cryofractured surface morphologies of PET/PA (60/40) prepared with various MWCNT contents. PA6 phase (a) 0, (b) 0.001, (c) 0.01, (d) 0.05, (e) 0.1, (f) 0.3, (g) 0.5, (h) 1, and (i) 2 phr.

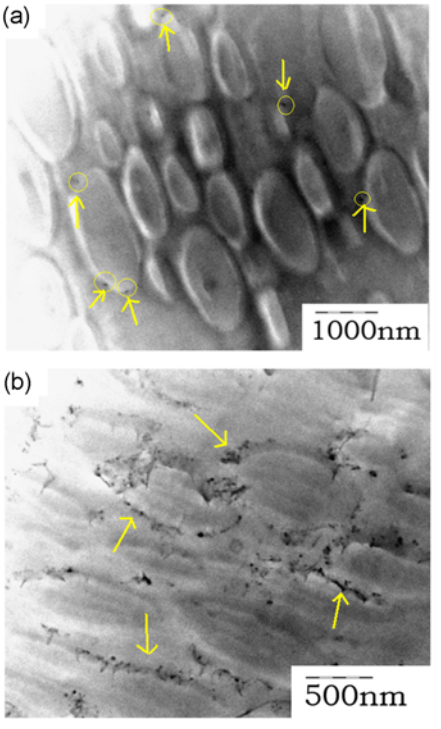

Figure 2. TEM micrographs of MWCNT-filled PET/PA6 (60/40) blend. (a) 0.01 and (b) 1 phr MWCNTs.

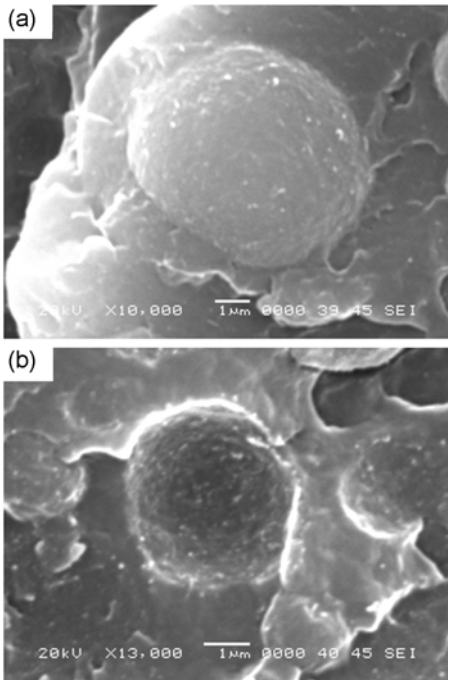

Figure 3. SEM micrographs of cryofractured surface morphologies of 0.5 phr MWCNTs filled with PET/PA6 (60/40) composite; (a) PA6 nodules and (b) PA6 cavities formed during cryofracture.

the images, MWCNTs are definitely present at the surface of the nodules and in the cavities, which demonstrates that the MWCNTs are localized at the interface between the two phases. This result is consistent with the morphology of the interface observed using TEM.

Classical thermodynamics is often used to predict the position of fillers in blends of immiscible polymers. In the equilibrium state, the location of CNTs in a polymer blend can be predicted by minimizing the interfacial energy. From Young's equation, the location of CNTs in an equilibrium state can be estimated by calculating the wetting coefficient (ω_a) [25] as follows:

$$\omega_a = \frac{\gamma_{CNT\text{-}PA6} - \gamma_{CNT\text{-}PET}}{\gamma_{PET\text{-}PA6}} \quad (1)$$

Where $\gamma_{CNT\text{-}PET}$, $\gamma_{CNT\text{-}PA6}$, and $\gamma_{PET\text{-}PA6}$ are the interfacial energies between the MWCNTs and the PET phase, the MWCNTs and the PA6 phase, and the PET and PA6 phases, respectively. MWCNTs will be preferentially located in the PET phase if the wetting coefficient (ω_a) is greater than 1, in the PA6 phase if ω_a is less than 1, and at the interface between the PET and PA6 phases if ω_a is between −1 and 1.

The interfacial energy can be calculated from the surface energies of the components. Two main approaches are used: the harmonic- and geometric-mean equations. The harmonic-mean equation is valid for interfaces between low-energy materials and the geometric mean equation is valid for interfaces between a low- and a high-energy material.

The harmonic mean equation is as follows:

$$\gamma_{PET\text{-}PA6} = \gamma_{PET} + \gamma_{PA6} - 4\left(\frac{\gamma^d_{PET}\gamma^d_{PA6}}{\gamma^d_{PET} + \gamma^d_{PA6}} + \frac{\gamma^p_{PET}\gamma^p_{PA6}}{\gamma^p_{PET} + \gamma^p_{PA6}}\right) \quad (2)$$

Geometric mean equation is as follows:

$$\gamma_{PET\text{-}PA6} = \gamma_{PET} + \gamma_{PA6} - 2(\sqrt{\gamma^d_{PET}\gamma^d_{PA6}} + \sqrt{\gamma^p_{PET}\gamma^p_{PA6}}) \quad (3)$$

Where γ_{PET} and γ_{PA6} are the surface tensions of the PET and PA6 phases, γ^d_{PET} and γ^d_{PA6} are the dispersive parts of the surface tensions of the PET and PA6 phases, and γ^p_{PET} and γ^p_{PA6} are the polar parts of the surface tensions of the PET and PA6 phases.

The values of the surface energy of the PET and PA6 phases in the melt state have been extrapolated from literature values for the surface energy of the PET and PA6 phases measured at 20 °C [26], which are detailed below and summarized in Table 1, on the basis of a simplified hypothesis that the polarity is independent of temperature.

Three papers concerning the wetting characteristics of MWCNTs were found in the literature [27-29]. The MWCNTs used in this study are unfunctionalized, therefore, they exhibit low surface polarity. Therefore, the surface energies of the MWCNTs used in this study are based on the surface energies evaluated by Barber *et al.*

The surface energies for the samples at 280 °C were evaluated based on the surface energies for samples at 20 °C, using the temperature coefficient for each component [29].

$$-d\gamma/dT = (11/9)(\gamma_0/T_c)(1 - T/T_c)^{2/9} \quad (4)$$

$$\gamma = \gamma_0(1 - T/T_c)^{11/9} \quad (5)$$

Where γ_0 is the surface tension at 0 K, T_c is the critical temperature, and T is the temperature of the polymer in K. For most polymers, T_c is about 1000 K.

Table 2 lists the surface energies of PET, PA6, and MWCNTs at 280 °C. The interfacial energies calculated using the harmonic and geometric mean equations for the samples at 280 °C are presented in Table 3. From the values presented in Table 4, the minimum interfacial energy predicts that MWCNTs should remain at the interface in PET/PA6

Table 1. Surface energy of polymer and MWCNTs at 20 °C [26,28]

Materials	Total surface energy ($mJ \cdot m^{-2}$)	Dispersive surface energy ($mJ \cdot m^{-2}$)	Polar surface energy ($mJ \cdot m^{-2}$)	Ref.
PET	44.6	35.6	9	[26]
PA6	46.5	32.5	14	[26]
MWCNTs	27.8	17.6	10.2	[28]

Table 2. Surface energy of polymer and MWCNTs at 280 °C

Materials	Total surface energy ($mJ \cdot m^{-2}$)	Dispersive surface energy ($mJ \cdot m^{-2}$)	Polar surface energy ($mJ \cdot m^{-2}$)
PET	25.5	20.4	5.1
PA6	26.6	22.3	8.0
MWCNTs	15.9	6	5.8

Table 3. Interfacial energies calculated using harmonic and geometric mean equations at 280 °C

Materials	Interfacial energy calculated based on harmonic mean equation ($mJ \cdot m^{-2}$)	Interfacial energy calculated based on geometric mean equation ($mJ \cdot m^{-2}$)
PET/PA6	−3.1	−3.46
PET/MWCNTs	11.91	8.29
PA6/MWCNTs	10.03	5.65

Table 4. Wetting coefficient evaluated based on harmonic and geometric mean equations

Materials	Wetting coefficient calculated based on harmonic mean equation	Wetting coefficient calculated based on geometric mean equation	Prediction
PET/PA6/ MWCNTs	0.6	0.76	Interface

systems. Thus, the preferential distribution of CNTs in PET/PA6 blends observed in this study is consistent with the interfacial energy.

Effect of MWCNTs on Rheological Behavior of PET/PA6 Blends

The rheological properties of the PET/PA6/MWCNT composites were investigated to further understand the internal structure of the composites. Figure 4 shows the effect of adding MWCNTs to the blends on the apparent viscosity of the blends measured at 260 °C. The apparent viscosity was converted from the melt-flow index (MFI) of the blends according to the ASTM D3835 standard as follows:

$$Viscosity = \frac{P\pi r^4}{8LQ} = \frac{Fr^4 t}{8R^2 LV} \quad (6)$$

Where P is the pressure due to ram (Pa), ram pressure is a pressure exerted on a body which is moving through a fluid medium. F is the magnitude of the force on ram (N), ram force is the total load applied by a ram, and numerically equal to the product of the line pressure and the cross-sectional area of the ram. r is the radius of the capillary (m), R is the radius of the barrel (m), L is the length of the capillary (m), Q is the flow rate, (m^3/s), V is the extruded volume (m^3), and t is the extrusion time (s).

The apparent viscosity of the PET/PA6 blends increased significantly with increasing MWCNT content. It was noted, however, that there was no clear change in the apparent viscosity of the blends containing up to 0.1 phr of MWCNTs in which phase inversion occurred. This result can be attributed to the formation of stronger interfacial interactions between the two immiscible PET/PA6 polymers due to MWCNTs at the interface. This in turn leads to the formation of interconnected or network-like structures of MWCNTs in the interfacial region, which restrains the long-range motion of polymer chains. The rheological behavior of the nanocomposites is proof for the localization of MWCNTs at the interface in the nanocomposite blends.

Effect of MWCNTs on Electrical Properties of PET/PA6 Blends

A percolated network structure formed in the polymer blend as a n ecessary c onsequence of MWCNT localization, which accompanied a decrease in the electrical resistivity of the polymer blend. Figure 5 shows the effect of adding MWCNT to the polymer blends on the electrical resistivity of the blends. From Figure 5, the MWCNTs had a negligible effect on the resistivity of the polymer blends containing small amounts of MWCNTs up to 0.1 phr. However, the SEM images reveal that the MWCNTs in the blends caused significant changes in the morphology of the phases. The conductive network was not formed probably because the MWCNT content in the blend was too low. The blend containing 0.3 phr of MWCNTs exhibited a distinct decrease in surface resistivity. The graph in Figure 5 shows a plateau for the blends containing 0.3-0.5 phr of MWCNTs, indicating that although there is not a significant decrease in the surface resistivity of the blends containing 0.3-0.5 phr of MWCNTs, the surface resistivity of the blends containing 0.3-0.5 phr of MWCNTs is obviously less than that of the blends containing less than 0.3 phr of MWCNTs. The composite blends containing more than 0.5 phr of MWCNTs exhibited a dramatic decrease in surface resistivity. This same trend is also demonstrated in the rheological properties of the composite blends: the surface resistivity of the blend containing 2 phr of MWCNTs decreased by 6 orders of magnitude to almost half the surface resistivity of the blend that did not contain any filled MWCNTs. These results when combined with the TEM images suggest that the interface-localized MWCNTs were connected in a network. Thus, a conductive MWCNT pathway was created, which was effective in decreasing the surface resistivity of the blends.

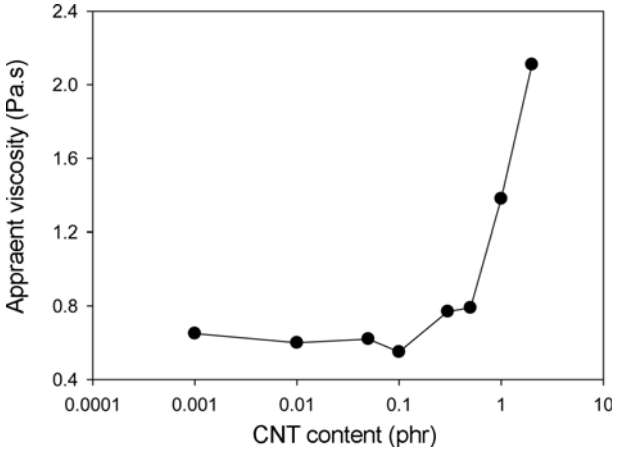

Figure 4. Apparent viscosity of PET/PA6/MWCNT blends measured at 260 °C.

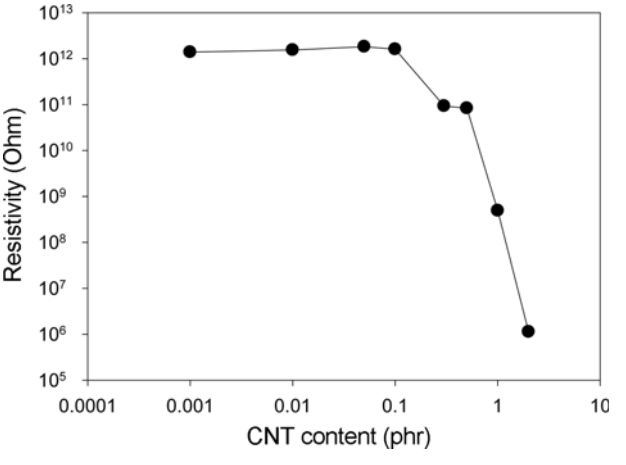

Figure 5. Electrical resistivity of PET/PA6 (60/40) versus MWCNT content.

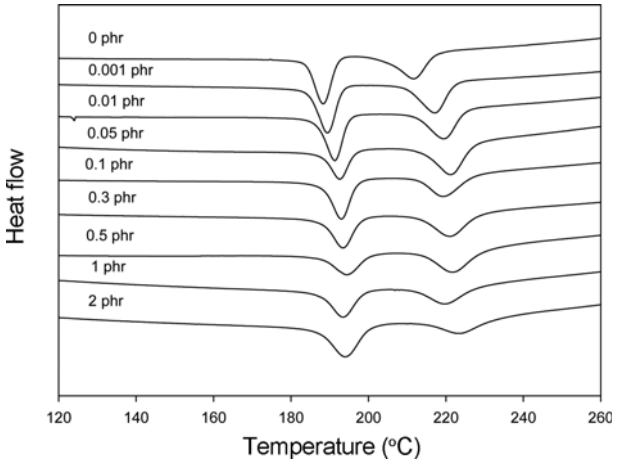

Figure 6. DSC thermograms for crystallization of PET/PA6/MWCNT nanocomposite blends (PET/PA6=60/40).

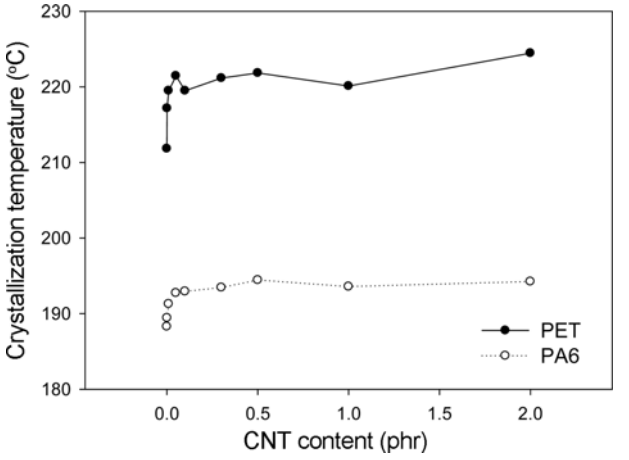

Figure 7. Crystallization temperature of PET/PA6 (60/40) versus MWCNT content.

Effect of MWCNTs on Thermal Properties of PET/PA6 Blends

The crystallization behaviors of the PET/PA6/MWCNT nanocomposites were examined through DSC measurements. Figure 6 and Figure 7 show the change in the crystallization temperature of PET/PA6 (60/40) with increasing MWCNT content in the blend. Both crystallization peaks for PET and PA6 could be separated because of a difference of about 30 °C in the crystallization temperature of the PET and PA6 phases. Adding MWCNTs, even in small amounts less than 0.1 phr, to the blends significantly increased the crystallization temperatures of both the PET and PA6 phases. This result implies that the crystallization rate of both the PET and PA6 phases was increased by adding MWCNTs. Although inorganic particles such as MWCNTs can act as nucleating agents in various polymer matrices and can accelerate crystallization [30], the increase in the crystallization temperature of both component polymers was not more noticeable for the blend containing 0.3 phr of MWCNTs because of the effect of saturated nucleation in blends containing high MWCNT contents.

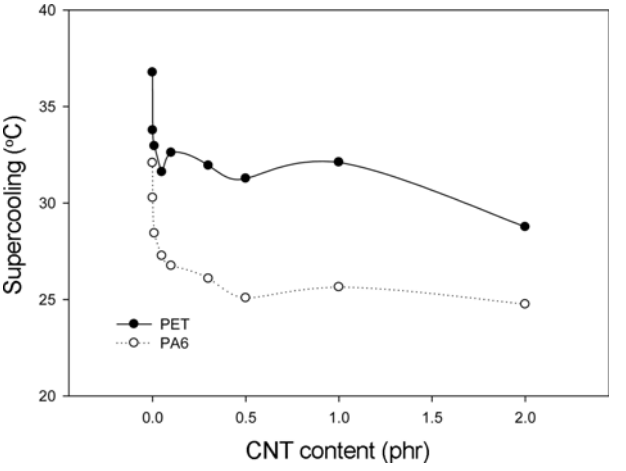

Figure 8. Changes of degree of supercooling according to the MWCNTs content.

Figure 8 represents the degree of supercooling of each polymer in the blends as a function of MWCNTs content. The parameter of melt crystallization temperature, T_{mc} is used to evaluate the nucleation behavior during polymer melt crystallization, with the higher the T_{mc}, then the easier it is for stable nuclei to be formed via the regular arrangement of polymer segments, so indicating a higher crystallizing ability. Since stable nuclei are difficult to form near the melting point, the degree of supercooling represents the thermodynamic 'drive' with the smaller the value of (T_m-T_{mc}), then the higher the crystallizing ability indicated. [31] From the Figure 8, it is notable that PA6 component crystallizes at smaller supercooling than PET in the blends, which implies that the crystallizing ability of PA6 is higher than that of PET.

Conclusion

Remarkable changes in morphology occurred when MWCNTs were added to PET/PA6 blends, that is, phase conversion occurred when a very limited amount of MWCNTs was added into the blends. The MWCNTs selectively located at the interface of the PET and PA6 phases, which just coincided with the calculated results for the wetting coefficient. A percolation threshold of about 0.3-0.5 phr carbon nanotubes was obtained during rheological and electrical resistivity testing. The interface-located MWCNTs were connected in a network, creating a conductive MWCNT pathway that was effective in decreasing the surface resistivity of the blends. The crystallization rate was found to be accelerated by the filler network of the MWCNTs.

Acknowledgement

This study was performed with the financial support of Kumoh National Institute of Technology.

References

1. S. *Iijima*, *Nature*, **354**, 56 (1991).
2. J.-W. An, D.-H. You, and D.-S. Lim, *Wear*, **255**, 677 (2003).
3. Y. Ding, H. Alias, D. Wen, and R. A. Williams, *Int. J. Heat and Mass Transfer*, **49**, 240 (2006).
4. C. Balazsi, B. Fenyi, N. Hegman, Z. Kover, F. Weber, Z. Vertesy, Z. Konya, I. Kiricsi, L. P. Biro, and P. Arato, *Composites*, *Part B* **37**, 418 (2006).
5. Z. Spitalsky, D. Tasis, K. Papagelis, and C. Galiotis, *Prog. Polym. Sci.*, **35**, 357 (2010).
6. H. Golestanian and M. Shojaie, *Comp. Mater. Sci.*, **50**, 731 (2010).
7. A. Sharma, B. Tripathi, and Y. K. Vijay, *J. Membr Sci.*, **361**, 89 (2010).
8. F. Tao, B. Nysten, A.-C. Baudouin, J.-M. Thomassin, D. Vuluga, C. Detrembleur, and C. Bailly, *Polymer*, **52**, 4798 (2011).
9. A. Cayla, C. Campagne, M. Rochery, and E. Devaux, *Synth. Met.*, **161**, 1034 (2011).
10. M. Gultner, A. Goldel, and P. Potschke, *Compos. Sci. Technol.*, **72**, 41 (2011).
11. P. Potschke, S. Pegel, M. Claes, and D. Bonduel, *Macromol. Rapid Commun*, **29**, 244 (2008).
12. L. Zhang, C. Wan, and Y. Zhang, *Compos. Sci. Technol.*, **69**, 2212 (2009).
13. L. Liu, Y. Wang, Y. Li, J. Wu, Z. Zhou, and C. Jiang, *Polymer*, **50**, 3072 (2009).
14. J.-F. Gao, D.-X. Yan, B. Yuan, H.-D. Huang, and Z.-M. Li, *Compos. Sci. Technol.*, **70**, 1973 (2010).
15. C.-M. Chang and Y.-L. Liu, *Canbon*, **48**, 1289 (2010).
16. D. Yan and G. Yang, *Mater. Lett.*, **63**, 1900 (2009).
17. S. Bose, A. R. Bhattacharyya, A. R. Kulkarni, and P. Potschke, *Compos. Sci. Technol.*, **69**, 365 (2009).
18. A.-C. Baudouin, D. Auhl, F. Tao, J. Devaux, and C. Bailly, *Polymer*, **52**, 149 (2011).
19. A.-C. Baudouin, J. Devaux, and C. Bailly, *Polymer*, **21**, 1341 (2010).
20. Y. Huang, Y. Liu, and C. Zhao, *J. Appl. Polym. Sci.*, **69**, 1505 (1998).
21. C. K. Samios and N. K. Kalfoglou, *Polymer*, **40**, 4811 (1999).
22. C. Qu, H. Yang, D. Liang, W. Cao, and Q. Fu, *J. Appl. Polym. Sci.*, **140**, 2288 (2007).
23. C. Qu, R. Su, Q. Zhang, R. Du, and Q. Fu, *Polym Int*., **57**, 139 (2008).
24. T. Serhatkulu, B. Erman, I. Bahar, S. Fakirov, M. Evstatiev, and D. Sapundjieva, *Polymer*, **36**, 2371 (1995).
25. S. Wu, "Polymer Interface and Adhesion", Marcel Dekker, New York, 1982.
26. http://www.surface-tension.de/solid-surface-energy.htm
27. S. Nuriel, L. Liu, A. H. Barber, and H. D. Wagner, *Chem. Phys. Lett.*, **404**, 263 (2005).
28. A. H. Barber, S. R. Cohen, and H. Daniel Wagner, *Phys. Rev. Lett.*, **92**, 186103/1 (2004).
29. O. Koysuren, S. Yesil, and G. Bayram, *J. Appl. Polym. Sci.*, **118**, 3041 (2010).
30. Z. Li, G. Luo, F. Wei, and Y. Huang, *Compos. Sci. Technol.*, **66**, 1022 (2006).
31. T. D. Fornes and D. R. Paul, *Polymer*, **44**, 3945 (2003).